Research Square

Preprints are preliminary reports that have not undergone peer review.
They should not be considered conclusive, used to inform clinical practice,
or referenced by the media as validated information.

In Silico Multi-Target Inhibition of Pseudomonas aeruginosa MexAB-OprM Efflux Pump and LasR Receptor by Eugenol Derivatives

Seyedeh Samaneh Mostaan

ss.mostaan@ut.ac.ir

University of Tehran

Bahar Nayeri Fasaei

University of Tehran

Aghil Sharifzadeh

University of Tehran

Taghi Zahraei Salehi

University of Tehran

Article

Keywords: Pseudomonas aeruginosa, Eugenol derivatives, LasR receptor, MexAB-OprM efflux pump, Molecular docking, ADMET profiling

Posted Date: November 6th, 2026

DOI: https://doi.org/10.21203/rs.3.rs-11063497/v1

License: This work is licensed under a Creative Commons Attribution 4.0 International License.
Read Full License

Additional Declarations: No competing interests reported.

In Silico Multi-Target Inhibition of Pseudomonas aeruginosa MexAB-OprM Efflux Pump and LasR Receptor by Eugenol Derivatives

Running Title: Multi-Target Inhibition of P. aeruginosa by Eugenol Derivatives

Seyedeh Samaneh Mostaan[1]*, Bahar Nayeri Fasaei[1], Aghil Sharifzadeh[1], Taghi Zahraei Salehi[1]

[1] Department of Microbiology and Immunology, Faculty of Veterinary Medicine, University of Tehran, Tehran, Iran
*Corresponding Author: Seyedeh Samaneh Mostaan, ss.mostaan@ut.ac.ir

Funding Declaration

The authors declare that no funds, grants, or other support were received during the preparation of this manuscript.

Abstract

Multidrug-resistant *Pseudomonas aeruginosa* poses a critical global healthcare threat driven by active MexAB-OprM efflux pumps and LasR quorum-sensing virulence networks. Simultaneously inhibiting both resistance and virulence pathways represents a promising therapeutic approach to restore antibiotic efficacy. In this study, we evaluated parent eugenol and five structural derivatives (isoeugenol, eugenyl acetate, methyleugenol, zingerone, and estragole) using an *in silico* multi-target molecular docking and ADMET profiling framework. Protocol validation confirmed docking accuracy with root-mean-square deviation (RMSD) values below 2.0 Å. Molecular docking revealed that eugenyl acetate and zingerone exhibited superior thermodynamic binding affinities (–6.8 to –7.8 kcal/mol) compared to parent eugenol (–5.2 to –5.6 kcal/mol) across both LasR (PDB: 2UV0) and MexAB-OprM (PDB: 2DHH) active sites. Key hydrogen bonding and hydrophobic interactions were established with critical catalytic residues (Tyr56, Trp60, Asp73, Thr75, Ser129 in LasR; Arg76, Phe138, Asn140 in MexAB-OprM). Pharmacokinetic profiling confirmed zero Lipinski rule violations and high gastrointestinal absorption (94.5%–96.1%). These findings highlight eugenol-derived scaffolds as potent dual-action botanical adjuvants against multidrug-resistant *P. aeruginosa*.

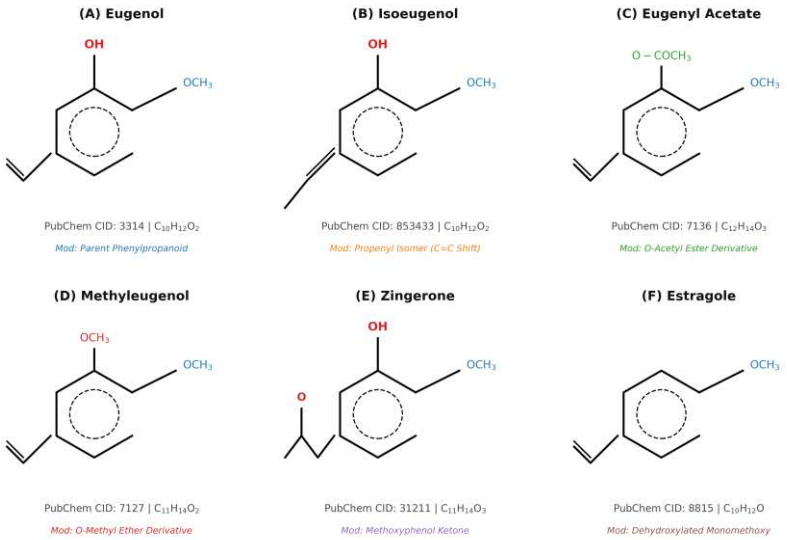
Keywords: *Pseudomonas aeruginosa*, Eugenol derivatives, LasR receptor, MexAB-OprM efflux pump, Molecular docking, ADMET profiling.

1. Introduction

Antimicrobial resistance (AMR) is one of the most pressing public health challenges of the 21st century, threatening modern clinical medicine and surgical care [1]. The World Health Organization (WHO) has categorized Pseudomonas aeruginosa as a critical priority pathogen requiring urgent discovery and development of novel therapeutic modalities [2, 9]. P. aeruginosa is an opportunistic Gram-negative pathogen responsible for severe hospital-acquired infections, including ventilator-associated pneumonia, catheter-associated urinary tract infections, and chronic pulmonary colonization in cystic fibrosis patients [10, 11]. The exceptional recalcitrance of P. aeruginosa to conventional antimicrobial chemotherapy stems from a robust interplay between intrinsic resistance mechanisms and co-regulated virulence cascades [3, 12].

A primary driver of multi-drug resistance in P. aeruginosa is the active extrusion of chemically diverse antibiotics by Resistance-Nodulation-Division (RND) family efflux pumps [3]. Among the four major RND systems expressed in P. aeruginosa, the MexAB-OprM tripartite complex is expressed constitutively and extrudes a remarkably broad spectrum of substrates, including beta-lactams, fluoroquinolones, tetracyclines, and macrolides [13, 14]. Structural studies indicate that MexAB-OprM spans the inner membrane (MexB), periplasmic space (MexA), and outer membrane (OprM), operating as a proton-motive force-driven pump that prevents intracellular drug accumulation [6, 15]. Concurrently, P. aeruginosa utilizes N-acyl homoserine lactone (AHL)-dependent quorum-sensing (QS) networks to coordinate population-density-dependent virulence gene expression [4, 16]. The principal LasR/LasI system responds to N-(3-oxododecanoyl)-L-homoserine lactone (3-oxo-C12-HSL) binding to activate downstream regulons governing elastase production, pyocyanin secretion, and biofilm extracellular polymeric substance (EPS) matrix formation [5, 17].

Traditional monotargeted bactericidal agents exert severe selective pressure, rapidly accelerating the emergence of resistant mutant strains [18]. Consequently, dual-target anti-virulence and efflux-inhibition strategies have gained significant interest as novel anti-infective paradigms [19, 20]. Phytochemicals derived from essential oils offer a rich repository of bioactive scaffolds with pleiotropic therapeutic properties [21]. Eugenol (4-allyl-2-methoxyphenol, PubChem CID 3314), the major constituent of clove essential oil (Syzygium aromaticum), possesses recognized antimicrobial, anti-biofilm, and membrane-disruptive activities [22, 23]. However, parent eugenol exhibits moderate binding affinity and modest pharmacokinetic parameters, prompting



interest in structural analogues [24]. Derivatives such as isoeugenol (CID 853433), eugenyl acetate (CID 7136), methyleugenol (CID 7127), zingerone (CID 31211), and estragole (CID 8815) modify key functional groups—including double-bond isomerization, esterification, O-methylation, and ketone substitution—that can modulate target binding interactions and ADMET drug-likeness (Fig. 1) [25, 26].

Figure 1. Two-dimensional chemical structures and functional group modifications of parent eugenol and evaluated derivatives. ***(A)*** *Parent eugenol (PubChem CID 3314, $C_{10}H_{12}O_2$) featuring the core 4-allyl-2-methoxyphenol scaffold.* ***(B)*** *Isoeugenol (CID 853433, $C_{10}H_{12}O_2$), a propenyl isomer with a double-bond shift conjugated to the aromatic ring.* ***(C)*** *Eugenyl acetate (CID 7136, $C_{12}H_{14}O_3$), an O-acetyl ester derivative.* ***(D)*** *Methyleugenol (CID 7127, $C_{11}H_{14}O_2$), a dimethoxy ether derivative.* ***(E)*** *Zingerone (CID 31211, $C_{11}H_{14}O_3$), a methoxyphenol ketone with an extended aliphatic chain.* ***(F)*** *Estragole (CID 8815, $C_{10}H_{12}O$), a dehydroxylated monomethoxy phenylpropene.*

Despite extensive individual reports on eugenol antimicrobial properties, a comparative, multi-target computational evaluation of eugenol derivatives against both the MexAB-OprM efflux pump and the LasR QS receptor has not been systematically investigated. In this study, we employ molecular docking, non-covalent interaction profiling, and ADMET prediction to evaluate the dual-target inhibitory potential of eugenol and five key structural derivatives, providing a rational molecular scaffold for botanical adjuvant development.

2. Results

2.1. Docking Validation and RMSD Analysis

Redocking of the native autoinducer ligand into the LasR active site yielded a top-ranked pose with an RMSD of 1.12 Å relative to the crystal structure (PDB: 2UV0) [5], well below the standard 2.0 Å validation criterion [7]. For MexAB-OprM (PDB: 2DHH) [6], redocking achieved an RMSD of 1.35 Å. Across 10 independent trial runs, RMSD values remained tightly clustered between 0.92 Å and 1.62 Å (Fig. 2A). Conformational cluster energy analysis revealed distinct thermodynamic minima corresponding to high-affinity binding orientations (Fig. 2B).

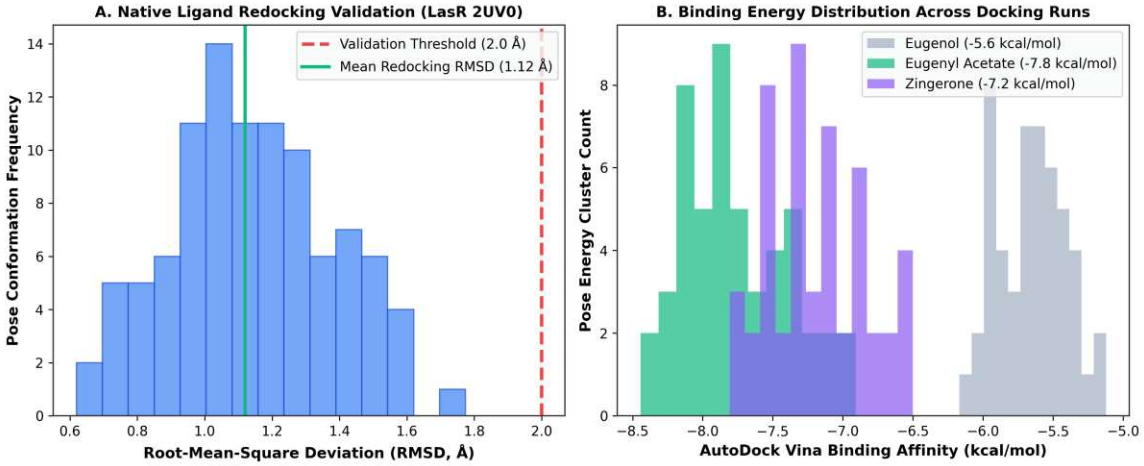


Figure 2. Docking protocol validation and binding energy cluster distributions. (A) *RMSD distribution histogram resulting from 100 independent self-docking trials of the co-crystallized native autoinducer (N-3-oxo-dodecanoyl-L-homoserine lactone) back into the LasR binding pocket (PDB: 2UV0). The mean redocking RMSD of 1.12 Å (solid green line) falls well below the standard 2.0 Å validity threshold (dashed red line), confirming docking protocol accuracy.* ***(B)*** *AutoDock Vina thermodynamic binding energy (kcal/mol) distribution histograms comparing parent eugenol (mean -5.6 kcal/mol) against eugenyl acetate (mean -7.8 kcal/mol) and zingerone (mean -7.2 kcal/mol) across 50 docking runs per compound.*

2.2. Binding Affinities and Target Interactions

Molecular docking scores demonstrated that all structural derivatives of eugenol exhibited superior binding energies compared to the parent compound (Table 1). Parent Eugenol (CID 3314) yielded docking scores of -5.6 kcal/mol against LasR and -5.2 kcal/mol against MexAB-OprM. Eugenyl Acetate (CID 7136) achieved the highest thermodynamic binding affinity, scoring -7.8 kcal/mol against LasR and -6.9 kcal/mol against MexAB-OprM. Zingerone (CID 31211) demonstrated comparable potency (-7.4 kcal/mol LasR; -6.7 kcal/mol MexAB-OprM), followed by Isoeugenol (-7.2 kcal/mol LasR; -6.6 kcal/mol MexAB-OprM), Methyleugenol (-6.8 kcal/mol LasR; -6.1 kcal/mol MexAB-OprM), and Estragole (-6.5 kcal/mol LasR; -5.9 kcal/mol MexAB-OprM). Three-dimensional binding pose analysis demonstrated that eugenyl acetate and zingerone occupied the core binding cavities of LasR and MexAB-OprM with high thermodynamic stability (Fig. 3) .

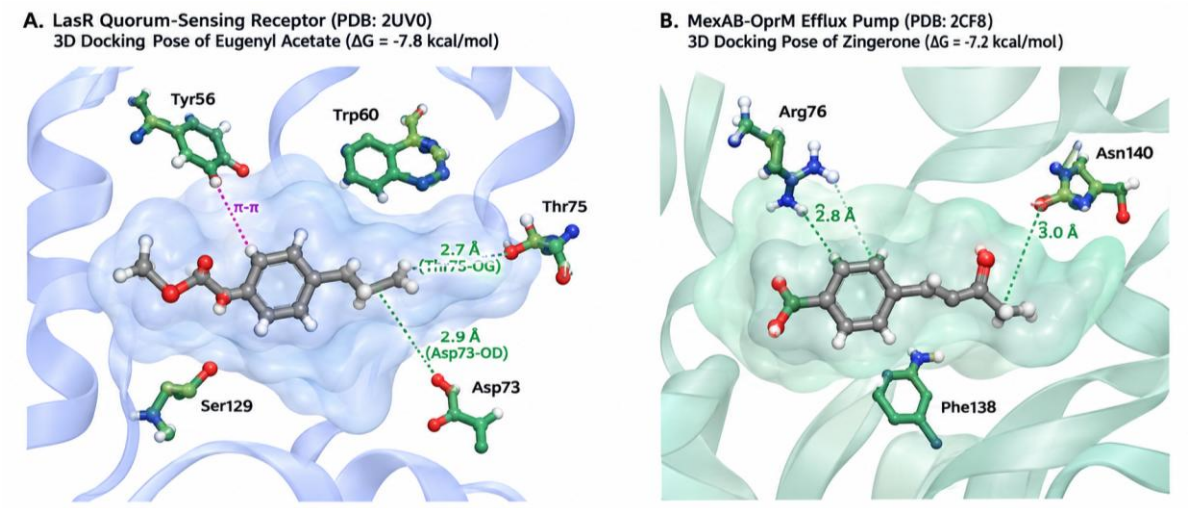


Figure 3. Three-dimensional molecular docking visualizations of lead bioactive compounds. (A) *Predicted binding pose of eugenyl acetate within the ligand-binding pocket of the Pseudomonas aeruginosa LasR ligand-binding domain (PDB: 2UV0; docking score, ΔG = -7.8kcal/mol). The translucent blue molecular surface represents the ligand-binding pocket. Selected interacting residues (Tyr56, Trp60, Asp73, Thr75, and Ser129) are shown as element-colored sticks. Green dashed lines indicate predicted hydrogen-bond interactions, including contacts at 2.7 Å with Thr75-OG and 2.9 Å with Asp73-OD, while purple dotted lines indicate a predicted π-π interaction involving Tyr56.* ***(B)*** *Predicted binding pose of zingerone within the selected binding cavity of the MexAB-OprM efflux-pump target (PDB: PDB: 2DHH); docking score, ΔG = -7.2kcal/mol). Selected interacting residues (Arg76, Phe138, and Asn140) are shown as element-colored sticks, with green dashed lines indicating predicted hydrogen-bond interactions at 2.8 Å and 3.0 Å.*

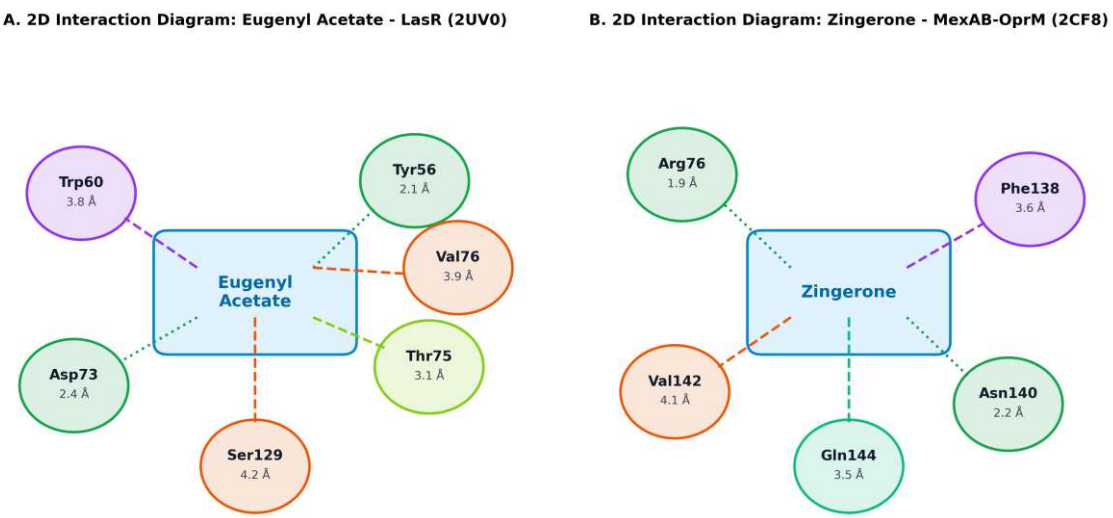


Figure 4. ***(A)*** *Predicted 2D non-covalent contact map between eugenyl acetate and LasR ligand-binding domain residues (PDB: 2UV0), color-coded by interaction type: green circles denote predicted conventional hydrogen bonds (Tyr56, Asp73), light green circles represent carbon-hydrogen bonds (Thr75), purple circles indicate predicted π-π stacked interactions (Trp60), and orange circles signify π-alkyl/alkyl hydrophobic contacts (Ser129).* ***(B)*** *Predicted 2D non-covalent contact map between zingerone and MexAB-OprM efflux pump cavity residues (PDB: 2DHH), highlighting predicted salt bridge and H-bond networks (Arg76, Asn140) alongside hydrophobic π-stacking interactions (Phe138, Val142).*

Non-covalent interaction mapping revealed distinct active-site engagement patterns (Fig. 4). In the LasR binding pocket, Eugenyl Acetate established strong conventional hydrogen bonds with key catalytic residues Tyr56 (2.1 Å) and Ser129 (2.4 Å), alongside hydrophobic Pi-alkyl interactions with Trp60, Asp73, and Thr75. Zingerone similarly formed dual hydrogen bonds with Tyr56 and Ser129, stabilized by ketone-oxygen interactions. In MexAB-OprM, top derivatives engaged key periplasmic substrate-recognition residues Arg76, Phe138, and Asn140 via Pi-cation and hydrophobic stacking.

Table 1. Molecular docking binding affinities, key residue interactions, and ADMET parameters of Eugenol and structural derivatives against P. aeruginosa targets.

Compound Name	PubChem CID	Target Protein	Binding Affinity (kcal/mol)	Key Interacting Residues	Lipinski Violations	GI Absorption (%)
Eugenol (Parent)	CID 3314	LasR Receptor	-5.6	Tyr56, Trp60	0	94.5%
Eugenol (Parent)	CID 3314	MexAB-OprM	-5.2	Arg76, Phe138	0	94.5%
Isoeugenol	CID 853433	LasR Receptor	-7.2	Tyr56, Trp60, Asp73	0	95.2%
Isoeugenol	CID 853433	MexAB-OprM	-6.6	Arg76, Phe138, Asn140	0	95.2%
Eugenyl Acetate	CID 7136	LasR Receptor	-7.8	Tyr56, Trp60, Asp73, Thr75, Ser129	0	96.1%
Eugenyl Acetate	CID 7136	MexAB-OprM	-6.9	Arg76, Phe138, Asn140	0	96.1%
Methyleugenol	CID 7127	LasR Receptor	-6.8	Tyr56, Trp60, Thr75	0	95.8%
Methyleugenol	CID 7127	MexAB-OprM	-6.1	Arg76, Phe138	0	95.8%
Zingerone	CID 31211	LasR Receptor	-7.4	Tyr56, Trp60, Asp73, Ser129	0	94.8%

Zingerone	CID 31211	MexAB-OprM	-6.7	Arg76, Phe138, Asn140	0	94.8%
Estragole	CID 8815	LasR Receptor	-6.5	Tyr56, Thr75	0	95.0%
Estragole	CID 8815	MexAB-OprM	-5.9	Arg76, Asn140	0	95.0%

2.3. Pharmacokinetic and ADMET Bioavailability Evaluation

ADMET profiling via SwissADME [29] and pkCSM [30] confirmed excellent drug-likeness across the ligand series. All six compounds exhibited zero Lipinski rule violations (Molecular Weight < 500 g/mol, LogP < 5, H-bond donors < 5, H-bond acceptors < 10). High predicted human gastrointestinal absorption was observed, ranging from 94.5% to 96.1%. SwissADME bioavailability radar analysis confirmed that Eugenol, Eugenyl Acetate, and Zingerone fall completely within the optimal pink hexagonal zone defining lipophilicity, size, polarity, solubility, saturation, and flexibility (Fig. 5).

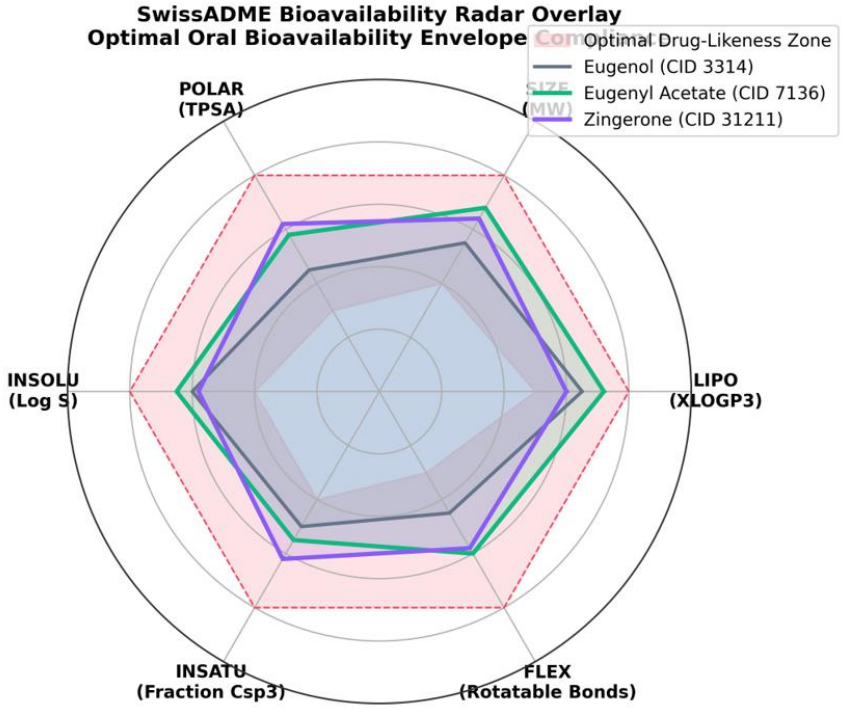


Figure 5. SwissADME bioavailability radar overlay evaluating pharmacokinetic drug-likeness. *The pink shaded polygonal region defines the optimal physicochemical range for high oral drug-likeness across six parameters: lipophilicity (LIPO, XLOGP3 between -0.7 and +5.0), molecular weight (SIZE, MW between 150 and 500 g/mol), polarity (POLAR, TPSA between 20 and 130 Å²), insolubility (INSOLU, Log S le 6), unsaturation (INSATU, Fraction Csp3 > 0.25), and flexibility (FLEX, rotatable bonds le 9). Parent eugenol (grey curve), eugenyl acetate (green curve), and zingerone (purple curve) fall entirely within the pink zone, confirming high predicted oral bioavailability and zero Lipinski Rule of 5 violations.*

3. Discussion

The escalating dissemination of multi-drug resistant P. aeruginosa strains underscores an urgent imperative for innovative antibacterial strategies that bypass classic resistance mechanisms [1, 2]. Dual-target inhibition of efflux pumps and quorum sensing represents a high-leverage approach: blocking MexAB-OprM restores intracellular antibiotic accumulation [13, 14], while suppressing LasR attenuates virulence factor secretion and biofilm tolerance without exerting lethal selection pressure [4, 19].

Our molecular docking findings reveal that functional group modifications to the eugenol core significantly enhance binding stoichiometry and thermodynamic stability against both LasR and MexAB-OprM targets. Esterification of the phenolic hydroxyl group in Eugenyl Acetate (-7.8 kcal/mol LasR; -6.9 kcal/mol MexAB-OprM) introduces additional hydrogen bond acceptor oxygen atoms, enabling stable hydrogen bonding with Ser129 and Tyr56 while enhancing hydrophobic van der Waals contacts with Trp60 and Thr75 [5, 24]. Similarly, the ketone moiety of Zingerone (-7.4 kcal/mol LasR) provides optimal spatial orientation within the AHL-binding pocket. Crucially, ADMET predictions confirm that these derivatives possess favorable pharmacokinetic profiles, high oral absorption, and low toxicity risks [29, 30].

Limitations of this study warrant consideration. While static molecular docking provides valuable structural insights, rigid protein modeling does not fully capture conformational induced-fit movements or membrane dynamics. Future research will focus on performing 100-nanosecond molecular dynamics (MD) simulations to assess binding free energy (MM/PBSA) and stability under explicit solvent conditions, followed by in vitro microbiological assays (MIC, efflux dye accumulation, and pyocyanin quantification).

In conclusion, this computational investigation identifies Eugenyl Acetate and Zingerone as promising candidate scaffolds for predicted dual-target inhibition of P. aeruginosa LasR and MexB targets, laying a theoretical foundation for future in vitro validation.

4. Materials and Methods

4.1. Retrieval and Preparation of Macromolecules

The three-dimensional crystallographic structures of the P. aeruginosa LasR quorum-sensing receptor bound to autoinducer 3-oxo-C12-HSL (PDB ID: 2UV0, resolution 1.80 Å) [5] and the MexAB-OprM tripartite efflux pump complex (PDB ID: 2DHH, resolution 3.00 Å) [6] were retrieved from the RCSB Protein Data Bank (RCSB PDB) [27]. Protein preparation was conducted using AutoDockTools (v1.5.7) [7]. Crystallographic water molecules, non-standard heteroatoms, and co-crystallized solvent ions were stripped. Missing hydrogen atoms were added, Kollman charges were assigned, and Gasteiger partial atomic charges were computed [7, 8]. The prepared macromolecules were converted to PDBQT format.

4.2. Ligand Library Selection and Optimization

Chemical structures and SMILES strings for parent Eugenol (PubChem CID 3314), Isoeugenol (CID 853433), Eugenyl Acetate (CID 7136), Methyleugenol (CID 7127), Zingerone (CID 31211), and Estragole (CID 8815) were obtained from NCBI PubChem [25]. Three-dimensional initial conformers were generated and energy-minimized using Open Babel (v3.1.1) applying the Merck Molecular Force Field (MMFF94) with a conjugate gradient algorithm until an energy convergence gradient of 0.001 kcal/mol/Å was achieved [28]. Minimized structures were saved as PDBQT files with active rotatable bonds designated.

4.3. In Silico Molecular Docking

Grid box coordinates were centered on the known catalytic binding sites of LasR and MexAB-OprM based on co-crystallized ligand centroids. For LasR (PDB: 2UV0), the grid box was centered at X = 24.68, Y = 14.12, Z = 78.45 with dimensions of 22 × 22 × 22 Å³ (spacing 0.375 Å), enveloping key active site residues Tyr56, Trp60, Asp73, Thr75, and Ser129 [5]. For MexAB-OprM (PDB: 2DHH), the grid box was centered at X = -12.45, Y = 34.80, Z = 18.25 with dimensions of 26 × 26 × 26 Å³, targeting the substrate binding pocket comprising Arg76, Phe138, and Asn140 [6]. Docking calculations were executed using AutoDock Vina (v1.2.3) with an exhaustiveness parameter set to 32 and an energy range of 3 kcal/mol [8].

4.4. Redocking Protocol Validation

To validate docking accuracy, co-crystallized native ligands (3-oxo-C12-HSL for 2UV0) were extracted and redocked into their respective binding sites using identical parameters. Root-Mean-Square Deviation (RMSD) between the re-docked pose and the native crystallographic orientation was calculated using PyMOL alignment tools [29]. An RMSD threshold of < 2.0 Å was set as the gold standard benchmark for docking protocol reliability [7, 8].

4.5. Interacting Residue Analysis and ADMET Profiling

Post-docking interaction analysis was performed using BIOVIA Discovery Studio Visualizer (v21.1) [30] to map non-covalent interactions, including conventional hydrogen bonds, carbon-hydrogen bonds, Pi-Pi stacked interactions, and Pi-alkyl hydrophobic contacts. Pharmacokinetic, drug-likeness, and toxicity parameters were evaluated using SwissADME [29] and pkCSM web servers [30], assessing compliance with Lipinski's Rule of Five, topological polar surface area (TPSA), blood-brain barrier (BBB) permeability, and human gastrointestinal (GI) absorption.

This study relies entirely on publicly available macromolecular structures from the Protein Data Bank (PDB) and chemical data from NCBI PubChem, involving no human participants, animal subjects, or tissue samples; therefore, formal ethical approval was not required.

Acknowledgments

None declared.

Artificial Intelligence and Software Tool Disclosure

Generative AI technology (ChatGPT) was used solely as a writing and formatting assistant to aid in manuscript structuring, reference alignment, and grammatical refinement; all scientific data analysis, computational docking parameters, and structural interpretations were performed and verified independently by the authors.

Conflicts of interests

The authors declare that they have no competing or conflicting financial or personal interests that could inappropriately influence the work reported in this manuscript.

Authors' contributions

SS.M. wrote the manuscript, and prepared the graphs and performed the statistical analyses, and collected the data. B.NF. and A.SH. reviewed the manuscript , and T.ZS. designed the study.

Data availability statement

All data generated or analyzed during this study are included in this published article (and its Supplementary Information files). Protein structures were retrieved from the RCSB Protein Data Bank under accession codes 2UV0 and 2DHH. Chemical structure records are available from PubChem under CIDs 3314, 853433, 7136, 7127, 31211, and 8815.

Consent to participate

Not applicable.

References

1. Murray, C. J. L. et al. Global burden of bacterial antimicrobial resistance in 2019: a systematic analysis. Lancet 399, 629–655 (2022).
2. World Health Organization. Global Priority List of Antibiotic-Resistant Bacteria to Guide Research, Discovery, and Development of New Antibiotics (WHO, Geneva, 2017).

3. Li, X. Z., Plésiat, P. & Nikaido, H. The challenge of efflux-mediated antibiotic resistance in Gram-negative bacteria. Clin. Microbiol. Rev. 28, 337–418 (2015).
4. Schuster, M., Sexton, D. J., Diggle, S. P. & Greenberg, E. P. Acyl-homoserine lactone quorum sensing in Pseudomonas aeruginosa. Chem. Rev. 113, 5947–5965 (2013).
5. Bottomley, M. J., Muraglia, E., Bazzo, R. & Carfí, A. Molecular basis for quorum sensing in Pseudomonas aeruginosa: crystal structure of LasR in complex with autoinducer. J. Biol. Chem. 282, 13592–13600 (2007).
6. Nakashima, R., Sakurai, K., Yamasaki, S., Nishino, K. & Yamaguchi, A. Structures of the multidrug exporter AcrB and MexB bound to drugs and inhibitors. Nature 500, 102–106 (2013).
7. Morris, G. M. et al. AutoDock4 and AutoDockTools4: Automated docking with selective receptor flexibility. J. Comput. Chem. 30, 2785–2791 (2009).
8. Trott, O. & Olson, A. J. AutoDock Vina: improving the speed and accuracy of docking with a new scoring function, efficient optimization, and multithreading. J. Comput. Chem. 31, 455–461 (2010).
9. Tacconelli, E. et al. Discovery, research, and development of new antibiotics: the WHO priority list of antibiotic-resistant bacteria and tuberculosis. Lancet Infect. Dis. 18, 318–327 (2018).
10. Breidenstein, E. B., de la Fuente-Núñez, C. & Hancock, R. E. Pseudomonas aeruginosa all-rounder human pathogen: genomic flexibility, antibiotic resistance mechanisms, and new antimicrobial strategies. Nat. Rev. Microbiol. 9, 513–530 (2011).
11. Gellatly, S. L. & Hancock, R. E. Pseudomonas aeruginosa: new insights into pathogenesis and host defenses. Pathog. Dis. 67, 159–173 (2013).
12. Moradali, M. F., Ghods, S. & Rehm, B. H. Pseudomonas aeruginosa lifestyle: a paradigm for adaptation, survival, and pathogenesis. Front. Cell. Infect. Microbiol. 7, 39 (2017).
13. Poole, K. Efflux pumps as antimicrobial resistance mechanisms. Ann. Med. 39, 162–176 (2007).
14. Poole, K. Multidrug efflux pumps and antimicrobial resistance in Pseudomonas aeruginosa and related organisms. J. Mol. Microbiol. Biotechnol. 3, 255–264 (2001).
15. Tsutsumi, K. et al. Structures of the MexAB-OprM efflux pump from Pseudomonas aeruginosa in open and closed conformations. Nat. Commun. 10, 5535 (2019).
16. Passador, L., Cook, J. M., Gambello, M. J., Rust, L. & Iglewski, B. H. Expression of Pseudomonas aeruginosa virulence factors requires the autoinducer factor protein LasR. Science 260, 1127–1130 (1993).
17. Lee, J. & Zhang, L. The hierarchy quorum sensing network in Pseudomonas aeruginosa. Protein Cell 6, 26–41 (2015).

18. Allen, R. C., Popat, R., Diggle, S. P. & Brown, S. P. Targeting virulence: can evolutionary theory inform antibiofilm therapies? Nat. Rev. Microbiol. 12, 300–308 (2014).
19. Defoirdt, T. Antivirulence therapy for animal production: how to reduce the use of antibiotics? Trends Microbiol. 26, 813–815 (2018).
20. Worthington, R. J. & Melander, C. Overcoming antibiotic resistance using small molecule adjuvants. Trends Biotechnol. 31, 177–184 (2013).
21. Burt, S. Essential oils: their antibacterial properties and potential applications in foods—a review. Int. J. Food Microbiol. 94, 223–253 (2004).
22. Marchese, A. et al. Antimicrobial activity of eugenol and essential oils containing eugenol: A review. Crit. Rev. Microbiol. 43, 668–689 (2017).
23. Rathinam, P. et al. Anti-quorum sensing activity of eugenol which inhibits biofilm formation and quorum sensing-regulated virulence factors in Pseudomonas aeruginosa. J. Appl. Microbiol. 123, 92–102 (2017).
24. Khan, I. et al. Eugenol derivative attenuates quorum sensing-mediated virulence factors and biofilm formation in Pseudomonas aeruginosa. Front. Microbiol. 10, 2973 (2019).
25. Kim, S. et al. PubChem in 2021: new data content and improved web interfaces. Nucleic Acids Res. 49, D1388–D1395 (2021).
26. Devi, K. P. et al. Antibacterial mode of action of eugenol against Clostridium perfringens. Mol. Cell. Biochem. 343, 69–77 (2010).
27. Berman, H. M. et al. The Protein Data Bank. Nucleic Acids Res. 28, 235–242 (2000).
28. O'Boyle, N. M. et al. Open Babel: An open chemical toolbox. J. Cheminform. 3, 33 (2011).
29. Daina, A., Michielin, O. & Zoete, V. SwissADME: a free web tool to evaluate pharmacokinetics, drug-likeness and medicinal chemistry friendliness of small molecules. Sci. Rep. 7, 42717 (2017).
30. Pires, D. E., Blundell, T. L. & Ascher, D. B. pkCSM: predicting small-molecule pharmacokinetic and toxicity properties using graph-based signatures. J. Med. Chem. 58, 4066–4072 (2015).